# Effective viscosity of active suspensions: Three-dimensional numerical modeling

Levan Jibuti* and Walter Zimmermann
*Theoretische Physik I, Universität Bayreuth, 95440 Bayreuth, Germany*

Salima Rafaï and Philippe Peyla
*Université Joseph Fourier and CNRS, F-38402 Grenoble, France*

A three-dimensional model is proposed for *Chlamydomonas Reinhardtii* swimming with a breaststroke-like beating of its two flagella. The model reveals unusual angular orbits of the active swimmer under a linear shear flow. Namely, the swimmer sustains orientation transiently across the flow when flagella plane is perpendicular to the shear plane, and amplify the shear-induced rotation along the flow. Such behavior is a result of the interplay between shear-induced deformation and swimmer's periodic beating motion that exerts internal torques on the torque-free swimmer. This particular behavior has some significant consequences on the rheological properties of the suspension that tends to confirm previous experimental results [Phys. Rev. Lett. 104, 098102 (2010)]. We calculated the intrinsic viscosity of the suspension with such isolated modeled microswimmers (dilute case) in shear flow using numerical simulations based on Rotne-Prager approximation. The results show an increased intrinsic viscosity for active swimmer suspensions in comparison to non-active ones in accordance with previous experimental measurements. A major enhancement of the active swimmer viscosity occurs due to the effectively extended shape of the deformable swimming cells. We also recover the experimentally observed shear thinning behavior.

**PACS numbers:** 47.50.Cd, 47.57.-s, 47.63.Gd, 47.63.ml

## I. INTRODUCTION

Self-propelled systems swimming on a microscopic scale have attracted growing interest over the last few years [1]. Typical examples of microswimmers include biological organisms: microalgae, bacteria, and sperm cells as well as artificial swimmers [2–4]. Usually, microswimmers are divided into two wide categories: "pullers" and "pushers." Pullers (e.g. *Chlamydomonas Reinhardtii* (*CR*)) pull the fluid toward them along their swimming direction while pushers (e.g. *Escherichia coli*) push the fluid back opposite to the swimming direction [1]. Designing controllable microswimmers, capable of detection *in vivo* and carrying a drug to treat and target certain localized diseases, is one of the most desired objectives in biophysics. Such a microswimmer should employ special tactics to overcome low Reynolds number constraints for locomotion [5] as well as control their swimming direction or cross-streamline migration [6] in the flow (e.g. Poiseuille flow in bloodstreams).

Another important field of growing interest involving microswimmers is the physics of active soft matter. Active fluids are suspensions of particles (or microorganisms) that transform the chemical energy of surrounding fluid or their stored energy into mechanical work by moving through a fluid, spinning or deforming and, as a result, significantly alter the macroscopic properties of the ambient fluid [7]. In this work, we concentrate on the study of such a property of complex active fluids. Namely, the rheological characteristics of *Chlamydomonas Reinhardtii* dilute suspension.

Despite recent keen interest, there are only a few experimental measurements of the effective viscosity of active suspensions. Sokolov and Aranson [8] measured the viscosity of pusher type bacterial suspension. They report strong decrease of the effective viscosity (up to a factor of 7). In a preceding study [9], some of the authors measured the viscosity of puller type unicellular motile microalgae (*Chlamydomonas Reinhardtii*) suspensions and found it significantly increased compared to suspensions containing the same volume fraction of dead cells. Suspensions of live microalgae also show a shear thinning behavior. In another experiment, Mussler *et al.* [10] confirmed the previous results using two different (Taylor-Couette and cone-plate) geometries and show that gravity does not play a role in the enhancement of the viscosity unlike of bottom-heavy *Chlamydomonas nivalis* suspension [11, 12].

Several theoretical works and numerical simulations have been done to predict the rheological behavior of active suspensions [13–16]. Saintillan used kinetic models for the extensional rheology of dilute active swimmer suspensions and predicted an enhancement of the viscosity for a puller type microswimmer suspension and reduction of the viscosity for a pusher type microswimmer suspension [13]. This prediction was confirmed recently by Gachelin *et al.* [12]. Similar behavior was predicted in the theoretical work of Hatwalne *et al.* [7], Haines *et al.* [17] and Heidenreich *et al.* [15] for swimmer suspensions. The models that unify both effects (enhancement of the viscosity for pullers and reduction for pushers) rely on an anisotropic orientation distribution of swimmers with a force dipole in the flow [13, 17]. Such an assumption is natural for the suspensions of pusher type bacteria that have a rod-like shape. However, it is not applicable for the non-gravitactic suspension of *CR* with nearly spher-

* levan.jibuti@uni-bayreuth.de

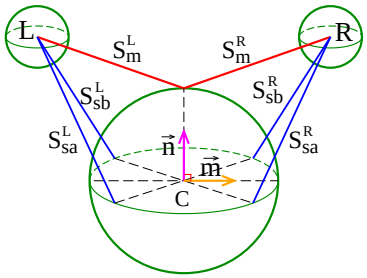


FIG. 1. The model swimmer consists of three beads connected by a set of Hookean springs. The unit vector $\vec{n}$ defines the swimming direction. The unit vector $\vec{m}$, together with $\vec{n}$, sets the flagellar beating plane. $L$ and $R$ respectively refer to the left and right flagella modeled as tiny spheres. The ratio of the radius between large and small beads is $R/r = 3$.

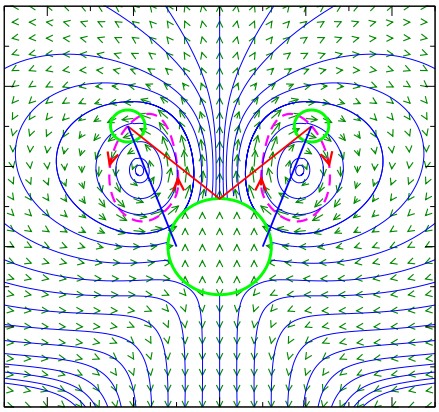

FIG. 2. The velocity field and streamlines around the model swimmer in fluid at rest averaged over one period of flagellar beating. The dashed close curves represent the orbits of each satellite beads with respect to the central bead. The swimmer moves back and forth during the period but moves forward with an average velocity $v = 53.76\mu m/s$.

ical body of $\sim 10\mu m$ diameter. Therefore, the origin of the viscosity enhancement in *CR* suspensions remains an open question. In this work, we address these questions, using the model that takes into account the flagella movement.

In many theoretical and numerical works, microswimmers are modeled as a permanent force dipole (or stresslet) [7, 13, 14, 18, 19]. Mehandia and Nott proposed a force triplet model for a biflagellate micro-organism [20]. Drescher *et al.* used a set of three Stokeslets to describe the time-averaged flow field of swimming *CR* [21]. The use a permanent force dipole to describe the swimmer activity is reasonable on long time scales. However, taking into account swimmer dynamics on short time scales (like periodic motion of flagella) appears to be crucial, when there is another time scale in the system (e.g. the shear rate).

In this paper, we proposed a three-beads model for *CR* swimming in three dimensions, involving the periodic breaststroke-like motion of flagella, and use it to study the microswimmer rheology and dynamics under the shear flow. Our model shares similarities with the three-sphere models for *Chlamydomonas,* recently developed in two dimensions by Bennett and Golestanian [22] and Friedrich and Jülicher [23]. In both works, authors used three equal-sized spheres, connected by a frictionless scaffold. Where, two spheres representing flagella are moving on the circular orbits. Here, we propose to elucidate the effect of motility on the rheology of quasi-spherical active particles, and we show that the three-dimensional treatment is crucial to identify the origin of it.

TABLE I. Model parameters

| | $\frac{R}{r}$ | $\frac{k_s}{k_m}$ | $\frac{\ell_{m0}}{R}$ | $\frac{\ell_{s0}}{R}$ | $\frac{A_m}{R}$ | $\frac{A_s}{R}$ | $\frac{\omega}{2\pi}$ | $\delta\varphi$ |
|---|---|---|---|---|---|---|---|---|
| active | 3 | 4/7 | 1.93 | 1.77 | 1.26 | 0.795 | $\pi/3$ | $50Hz$ |
| inactive | 3 | 0 | 1.93 | - | - | - | - | - |

## II. THREE-BEADS MODEL FOR THE BIFLAGELLATE GREEN ALGAE

We propose a simple three-dimensional model for biflagellate algae *Chlamydomonas Reinhardtii,* which retains most of the swimming characteristics of the prototype swimmer cell. The model swimmer consists of three beads: one central bead with radius $R$ representing the body of the swimmer linked to two satellite smaller beads with radius $r$ representing the flagella of *CR*. The radius ratio of the central and the satellite beads is chosen as $R/r = 3$. Each of the two satellite beads is connected to the central bead with three Hookean springs [Fig. 1]. The main springs ($S_m^L$ and $S_m^R$), together with the small beads, mimic the flagella. While the supporting springs ($S_{sa}^L$, $S_{sb}^L$, $S_{sa}^R$ and $S_{sb}^R$) are used to hold small beads in three dimensions, and for assisting to make breaststroke-like circular motion. Two supporting springs together with the main spring are necessary to keep the small beads in stable mechanical equilibrium in three-dimensional space. In the case of single supporting spring, the small beads would move freely along the direction perpendicular of two acting spring forces. The two perpendicular unit vectors, $\vec{n}$ and $\vec{m}$, determine the orientation and the swimming direction of the swimmer. More precisely, the vector $\vec{n}$ is used to determine the fastening point, where main springs are attach to the central bead. Meantime, $\vec{n}$ indicate the swimming direction of isolated swimmer during the synchronized beating motion of small beads. The vector $\vec{m}$ (perpendicular of $\vec{n}$) is used to determine the rest of the fastening points, where supporting springs are attach to the central bead. Then $\vec{n} \times \vec{m}$ is a normal vector of the "flagella plane" where small beads are orbiting. The supporting springs fastening points to the central bead create a square on the central bead's equatorial plane (with diagonals of length

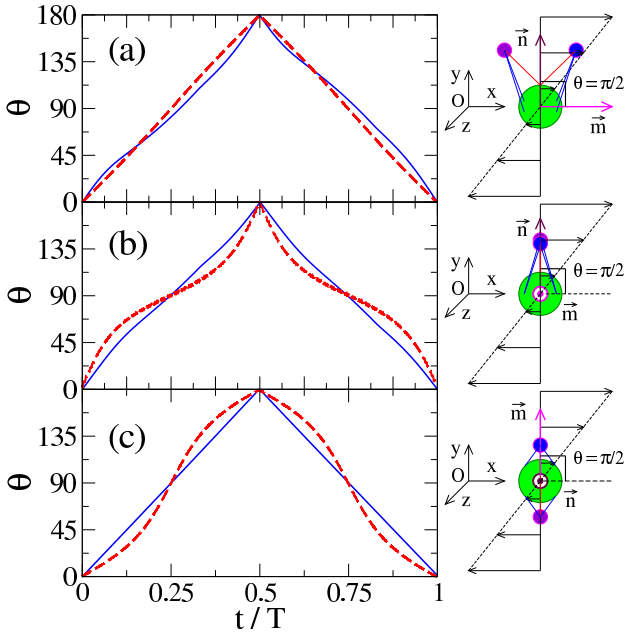


FIG. 3. Orientation angles of swimmers in the shear flow. (a) $\vec{n}$ (swimming direction) and $\vec{m}$ ($\vec{n} \times \vec{m}$ is a normal of the flagella plane) both are in the shear plane $xy$. (b) $\vec{n}$ is in the shear plane while $\vec{m}$ is parallel to $z$ (perpendicular to the shear plane). (c) $\vec{m}$ is in the shear plane while $\vec{n}$ is parallel to $z$-axis. For (a) and (b) $\theta$ is the angle between $\vec{n}$ and $x$-axis, while for (c) $\theta$ is the angle between $\vec{m}$ and $x$-axis. On the abscissa, $T$ is the swimmer's tumbling period in the shear flow, and it differs for each curve [see Table III]. Solid curves correspond to the inactive swimmer, dashed curves refers to the active swimmer.

$2R$). The vector $\vec{n}$ is normal to that square, and two sides are parallel to $\vec{m}$). In order to achieve swimming, each spring represents the time-dependent harmonic oscillators with given frequency $\omega$. Namely, equilibrium lengths of each Hookean springs are time-dependent harmonic functions: $\ell_m^{L,R}(t) = \ell_{m0}^{L,R} + A_m^{L,R} cos(\omega t + \varphi_m^{L,R})$, $\ell_{sa}^{L,R}(t) = \ell_{sa0}^{L,R} + A_{sa}^{L,R} cos(\omega t + \varphi_{sa}^{L,R})$ and $\ell_{sb}^{L,R}(t) = \ell_{sb0}^{L,R} + A_{sb}^{L,R} cos(\omega t + \varphi_{sb}^{L,R})$. Each spring applies equal and opposite forces on corresponding small bead and the central bead. Springs also exert torque on the central bead since the fastening points are on the surface of the central bead. However, total force and torque exerted by the model swimmer on the fluid are identically zero at every instant.

Total of 25 general spring parameters defines the swimming characteristics. Those parameters are: the stationary parts of equilibrium lengths ($\ell_{m0}^{L,R}$, $\ell_{sa0}^{L,R}$, $\ell_{sb0}^{L,R}$), the amplitudes ($A_m^{L,R}$, $A_{sa}^{L,R}$, $A_{sb}^{L,R}$), the phases ($\varphi_m^{L,R}$, $\varphi_{sa}^{L,R}$, $\varphi_{sb}^{L,R}$) of equilibrium lengths oscillation, the oscillation frequency $\omega$ and the spring constants ($k_m^{L,R}$, $k_{sa}^{L,R}$, $k_{sb}^{L,R}$). This number can be considerably reduced by using symmetry arguments. If we consider a mirror-symmetric swimmer then parameters for the left and the right beads must be identical. If the swimmer is not spinning around its swimming direction ($\vec{n}$), the supporting springs parameters for [$a$] and [$b$] springs are equal. If we take into account that only the phase shift between the main and the supporting springs ($\delta\varphi = \varphi_s - \varphi_m$) are important rather than the phases itself, this leaves only eight independent parameters ($\ell_{m0}$, $\ell_{s0}$, $A_m$, $A_s$, $\delta\varphi$, $\omega$, $k_m$ and $k_s$). When both the left and the right beads are activated by symmetric oscillators with the given parameters, beads are orbiting on their ellipse-like path, similar to the way a human swimmer uses his or her arms. The model swimmer moves forward (along $\vec{n}$) in a zigzagging manner, similar to the puller $CR$ [see supplementary material]. We recover the experimentally observed zigzagging swimming of $CR$ that occurs at the beating frequency [24]. Figure 2 shows the orbits of small beads with the velocity field and the streamlines averaged over the period of small beads rotation. The left bead is orbiting counter-clockwise and the right bead is orbiting clockwise. Along the paper, the spring parameters for the mirror-symmetric puller swimmer are chosen as follow: $\ell_{m0} = 1.93R$; $\ell_{s0} = 1.77R$; $A_m = 1.26R$; $A_s = 0.795R$; $\delta\varphi = \pi/3$; $\omega = 2\pi \cdot 50Hz$ and $k_m/k_s = 7/4$ [see Table I]. Such a choice of the spring parameters is not unique. Changing those parameters, one can adjust trajectories of the small beads (shape, size, position with respect of the central bead). We choose a set of spring parameters that reproduce the swimming characteristics of the $CR$ more closely. The swimming velocity for the model swimmer with the chosen parameters (averaged over the period of small beads rotation $T_b = 2\pi/\omega = 1/50s$) is $\vec{v} = 10.752R\,s^{-1} \cdot \vec{n} = 53.76\mu m/s \cdot \vec{n}$. Here, the radius of swimmer body (central bead radius) is $R = 5\mu m$. Note that if spring parameters are chosen in such way that ($k_m/k_s < 1$ and $\delta\varphi \sim \pi$), then small beads orbits are reversed, and the swimmer moves backward (along $-\vec{n}$) like a pusher. If there is any asymmetry between left and right in the spring's parameters, then swimming is inefficient, swimmer is deviating along $\vec{n}$ and moves on a curved trajectory. If an asymmetry is between the supporting springs [$a$] and [$b$] of one of (or both) small beads, the swimmer is spinning around its swimming direction. In that way, our model can describe more complicated behaviors sometimes found for $CR$ [25]. However, here we restrain ourselves to the most simple case. In order to achieve a fast and efficient swimming for our model swimmer, it appears that a symmetric and synchronous beating is required, similar to the prototype swimmer cell. Breaking the symmetry between left and right beads orbiting results in swimmer rotation in the $nm$ plane. If needed, we use only the phase difference ($\Delta\varphi = \varphi_m^L - \varphi_m^R$) between the oscillators of the left and right beads as a mechanism of swimmer rotation. If $\Delta\varphi < 0$ the swimmer rotates clockwise, or if $\Delta\varphi > 0$ the swimmer rotates counter-clockwise.

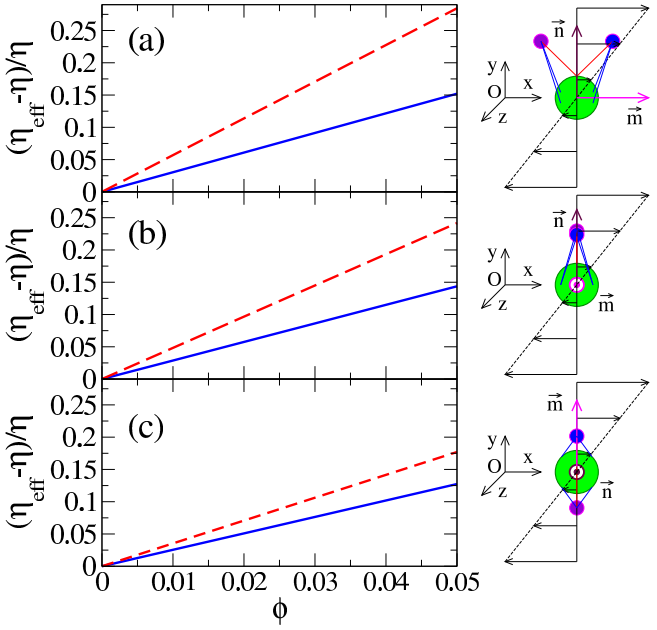


FIG. 4. The relative effective viscosity of dilute microswimmer suspension for three different orientations of swimmer flagella plane in the shear flow: (a) $\vec{n}$ and $\vec{m}$ both are in the shear plane $xy$; (b) $\vec{n}$ is in the shear plane, $\vec{m}$ is parallel to $z$; (c) $\vec{m}$ is in the shear plane, $\vec{n}$ is parallel to $z$. Solid lines correspond to an inactive swimmer, dashed lines corresponds to an active swimmer.

## III. THE INTRINSIC VISCOSITY OF THE MICROSWIMMER SUSPENSION

Now, we would like to understand how the swimming activity of *CR* cells affects the macroscopic properties of the suspension like its effective viscosity. We focus on a single swimmer contribution to the effective viscosity (i.e. in the dilute case) independently of hydrodynamic interactions among swimmers and consequently we neglect collective effects. We consider a microswimmer *CR*, which is approximately spherical in shape with $10\mu m$ diameter, swimming in a fluid at very low Reynolds number ($Re = \rho v R/\eta \sim 2.5 \times 10^{-4}$). Therefore, the inertial forces as well as the Brownian noise can be neglected. The Stokes equation governs hydrodynamics [26]. We consider the swimmer in the simple shear flow: $\vec{v} = (\dot{\gamma}y,\ 0,\ 0)$, where $\dot{\gamma}$ is the shear rate.

In a dilute suspension of rigid particles, where average distances between particles are large enough to neglect hydrodynamic interactions, the increase of effective viscosity is proportional to the concentration of the suspended particles,

$$\eta_{eff} = \eta(1 + \alpha\phi). \tag{1}$$

Here $\eta$ is the solvent viscosity, $\phi$ is the volume fraction and $\alpha$ is a proportional coefficient known as intrinsic viscosity. For rigid spherical particles, $\alpha = 5/2$ is known as Einstein's intrinsic viscosity [27]. In general, the intrinsic viscosity is defined as

$$\alpha = \lim_{\phi\to 0} \frac{\eta_{eff} - \eta}{\eta\phi}. \tag{2}$$

TABLE II. Intrinsic viscosity

| | $\alpha$ inactive | $\alpha$ active |
|---|---|---|
| $\vec{n}\angle xy;\ \vec{m}\angle xy$ | 3.0 | 5.7 |
| $\vec{n}\angle xy;\ \vec{m}\parallel z$ | 2.9 | 4.8 |
| $\vec{m}\angle xy;\ \vec{n}\parallel z$ | 2.5 | 3.5 |
| all configurations | 2.7 | 4.4 |
| experimental [9, 10] | $2.5 \pm 0.1$ | $4.5 \pm 0.2$ |

TABLE III. Period of tumbling

| | $T/T_b$ inactive | $T/T_b$ active |
|---|---|---|
| $\vec{n}\angle xy;\ \vec{m}\angle xy$ | 145.8 | 126.0 |
| $\vec{n}\angle xy;\ \vec{m}\parallel z$ | 144.9 | 166.3 |
| $\vec{m}\angle xy;\ \vec{n}\parallel z$ | 127.1 | 149.5 |

For the intrinsic viscosity of the modeled microswimmer suspension, the stress tensor ($\sigma_{ik}$) is averaged in a volume containing the single microswimmer submitted to the shear flow ($\overline{\sigma}_{ik} = 1/V \int \sigma_{ik} dV$). The volume integral is reduced to the surface integral that allows to avoid the difficulty with the calculation of the stress tensor inside the particle [28, 29]. Any simple closed surface can be selected for integration while it contains the swimmer (or passive particle). Then the intrinsic viscosity is estimated as follows,

$$\alpha = \frac{1}{2\eta E_{ik} V_0} \oint \{\sigma_{ij} x_k l_j - \eta(v_i l_k + v_k l_i)\}\, dA. \tag{3}$$

Here $V_0 = 4/3\pi(R^3 + 2r^3)$ is the volume of the suspended model swimmer, $\vec{l}$ is the unit outward normal vector of a closed surface, $\vec{x}$ is the position vector from the center of the swimmer, and $E_{ik} = \frac{1}{2}(\frac{\partial U_i}{\partial x_k} + \frac{\partial U_k}{\partial x_i})$ is the rate of strain tensor, where $\vec{U}$ is the mean (bulk averaged) velocity. In simple shear flow ($\vec{v} = (\dot{\gamma}y,\ 0,\ 0)$) after averaging over all possible orientations of the swimmer's tumbling during a full period, the only non-zero components of the strain tensor are $E_{12} = E_{21} = \dot{\gamma}/2$. In the case of a passive rigid sphere (with a radius $R$ and volume $V_0 = 4/3\pi R^3$) the exact velocity and pressure fields are known analytically. Moreover, the calculation of the surface integral [Eq. 3] recovers Einstein's intrinsic viscosity ($\alpha = 5/2$).

In the experiments [9, 10], significant enhancement of the effective viscosity was reported for the active cell suspensions. The hydrodynamic interactions among swimmers, as well as interaction between swimmers and walls [30], may play an important role for concentrated suspensions. Our analysis based on the single swimmer does not include those effects and is limited for very dilute suspension ($\phi < 0.05$). However, we compare numerically calculated intrinsic viscosity ($\alpha$) for dilute suspensions to the experimental value $\alpha_{exp}$ [9] estimated from a fit

done with Krieger and Dougherty's law [31] with different concentrations. In the following, the model microswimmer with harmonic springs that imitates the swimming *CR* will be referred as "active swimmer." Meanwhile, we consider a modified object "inactive swimmer" that mimics the inactive or dead cell of *CR*. For the inactive object the supporting springs ($S^L_{sa}$, $S^L_{sb}$, $S^R_{sa}$ and $S^R_{sb}$) are removed [Fig. 1] as well as the time-dependent parts of the remained main springs ($A_m = 0$). In such a flexible object, the small beads connected to the central bead by single springs are allowed to move freely in the vicinity of the central bead due to an external flow. However, small beads cannot separate much far (than $\ell_{m0}$) from the central bead, and also are restricted not to penetrate it, similar to the flagella of dead *CR* cell.

An exact analytical calculation of the intrinsic viscosity of the presented model microswimmer suspension (unlike the passive sphere suspension) requires immense effort and could be very complicated. We choose to perform numerical simulations based on generalized Rotne-Prager approximation [32, 33] to calculate the dynamics, as well as the intrinsic viscosity of the corresponding suspension submitted to an unbounded shear flow.

## IV. RESULTS AND DISCUSSION

The intrinsic viscosity of the model microswimmer suspension, calculated at a given instant, is independent of the choice of a closed surface for integration in (3) (while it encloses the swimmer). However, the intrinsic viscosity strongly depends on the relative positions of small beads on their orbits. It also depends on the orientation of swimmer and swimmer's flagella plane with respect to the flow direction and the shear plane. The viscosity averaged over the orbital period of small beads ($T_b$) smoothly change during swimmer's tumbling in a shear flow. Hence, to estimate macroscopic quantity of suspension - the viscosity - we average it within the tumbling period ($T$) in a shear flow. The tumbling period differs for swimmers of different initial orientation [see Table III]. In dilute suspensions where one can neglect a collective behavior, we assume that any initial orientation of swimmers is equally probable (this may not be true for gravitactic microswimmers). Therefore, before comparing our numerical results concerning intrinsic viscosity to the experiments, we take the ensemble average of different realization of swimmer's orientation with respect to the flow direction and the shear plane.

For the evaluation of the intrinsic viscosity, we choose the shear rate $\dot{\gamma} = 5s^{-1}$, corresponding to the value used in the experiments [9, 10]. For the active swimmer suspension, we obtain the intrinsic viscosity $\alpha = 4.4$ while for inactive swimmer suspension $\alpha = 2.7$. The intrinsic viscosity of the active swimmer suspension is consistent with the experimentally measured viscosity ($\alpha_{exp} = 4.5 \pm 0.2$) [9] and ($\alpha_{exp} = 4.5 \pm 0.17$) [10]. For inactive swimmer suspension, the numerically calculated intrinsic viscosity is slightly larger compared to the experimental value $\alpha_{exp} = 2.5 \pm 0.1$ [9]. Nevertheless, the agreement between numerical values of $\alpha$ and the experiments is good given the fact that in the experiments, $\alpha$ is indirectly extracted from a fit of the data by a semi-empirical law.

It is useful to consider some particular orientations of the swimmer with respect to the shear frame, to identify the origin of the viscosity enhancement. In the first configuration the swimmer is in the shear plane ($xy$, where $x$ is the flow direction and the flow changes along $y$). In other words, $\vec{n}$ (swimming direction) and $\vec{m}$ both are in the shear plane. In such a configuration, the swimmer is tumbling along $z$, and both $\vec{n}$ and $\vec{m}$ remains in the shear plane. In the case of active swimmers, intrinsic viscosity is $\alpha = 5.3$ [see Fig. 4(a)] while for inactive swimmers $\alpha = 3.0$. Besides that, the tumbling angular velocity in the shear flow for an active swimmer is surprisingly flat compared to the one of an elongated object [34] [see Fig. 3(a)]. The tumbling periods of the swimmers differ either it is active or inactive: for the inactive swimmer $T \simeq 146T_b$ and for the active swimmer $T \simeq 126T_b$.

Note that the tumbling period for a single sphere in the same shear flow will be $T = 2\pi/|\omega| = 4\pi/\dot{\gamma} \simeq 126T_b$.

A more unexpected orbit has been found for the active swimmer when $\vec{n}$ is in the shear plane and $\vec{m}$ is parallel to $z$ (perpendicular to the shear plane). The active swimmer rotates slower when $\vec{n}$ is aligned along $\pm y$ ($\theta \sim \pi/2$) and rotates faster when $\vec{n}$ is parallel to the flow ($\theta \sim 0$ or $\theta \sim \pi$), [see dashed curve on Fig. 3(b)]. Such behavior is opposite to the one for an elongated object in a shear flow. In a given configuration, the tumbling period for the inactive swimmer is $T \simeq 145T_b$, and the active swimmer $T \simeq 166T_b$. Drastic change of the active swimmer's orbit contributes to the viscosity enhancement, compared to the passive swimmer [see Fig. 4]. For the active swimmer suspension $\alpha = 4.8$; while $\alpha = 2.9$ for the inactive swimmer suspension [see Table II].

In another configuration of the swimmer considered here, $\vec{m}$ is in the shear plane and $\vec{n}$ is along $z$, the active swimmer is tumbling on usual Jeffery's-like orbit [see Fig. 3(c)]. The tumbling period for the inactive swimmer is $T \simeq 127T_b$, while for the active swimmer $T \simeq 150T_b$. For the active swimmer suspension $\alpha = 3.5$, and for the inactive swimmer suspension $\alpha = 2.5$ [see Fig. 4(c)]. In the case of any other arbitrary orientations of swimmer with respect to the shear plane, the effective viscosity smoothly changes between the corresponding configurations discussed here.

The contribution of swimmer's activity to the enhancement of the suspension viscosity is important when the swimming direction is in the shear plane, and the flagella plane is perpendicular to the shear plane [Fig. 4(b)]. The origin of the enhancement of the viscosity is the drastic difference in angular velocity of the swimmer [Fig. 3(b)]. The springs with time-dependent equilibrium lengths, in combination with the shear flow, exerts a torque on the central bead which changes the angular orbit of active

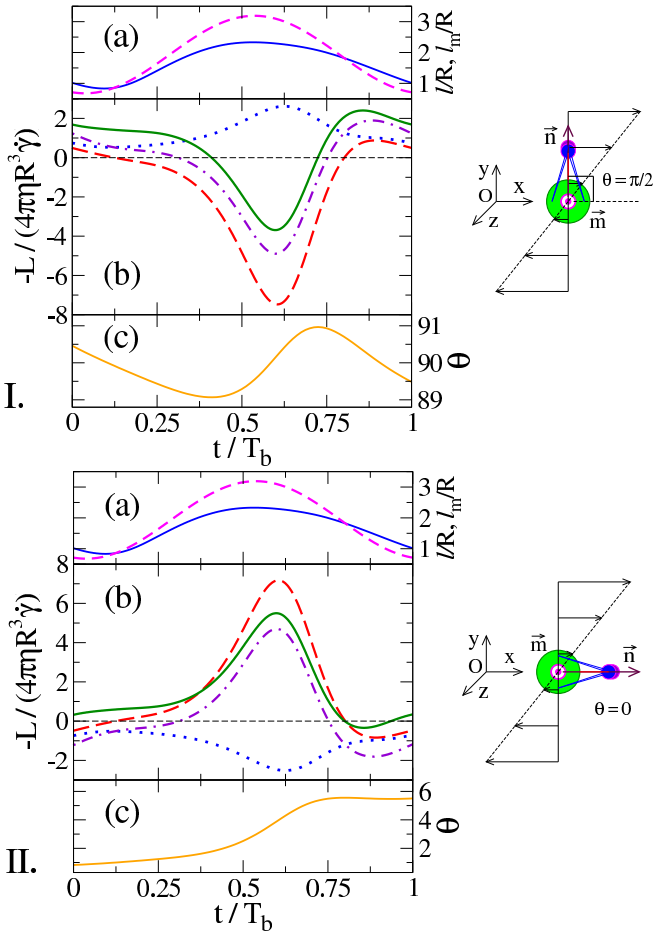


FIG. 5. (a) Actual length of main springs (solid curve) and the time-dependent equilibrium length of main springs (dashed curve) during the orbital period of small beads ($T_b$). (b) The contribution of main springs (dashed curve), supporting springs (dotted curve) and all spring together (dashed-dotted curve) to the relative angular velocity of the swimmer. Solid curve (b) shows the total relative angular velocity of the swimmer. (c) Orientation angle of the swimmer in the shear flow. The flagella plane ($\vec{n}\vec{m}$) is perpendicular to the shear plane ($xOy$). I. Swimming direction is perpendicular to the flow direction ($\vec{n} \parallel y$; $\vec{m} \parallel z$). II. Swimming direction is parallel to the flow direction ($\vec{n} \parallel x$; $\vec{m} \parallel z$).

swimmer. Naturally, springs also exert an equal and opposite torque on the fluid, such that, the total torque and force exerted by swimmer on the fluid is identically zero. When a mirror-symmetric model swimmer swims without an external flow, each spring exert a torque on the central bead, but the sum of the torques exerted by all springs is zero and swimmer moves without rotation.

Figure 5(b) shows the contribution separately of main springs, supporting springs and all springs together to the swimmer's rotation during the orbital period of small beads. Two configurations are considered when the flagella plane is perpendicular to the shear plane, and the swimming direction is perpendicular (I) or parallel (II) to the flow. The vertical axis shows the angular velocity

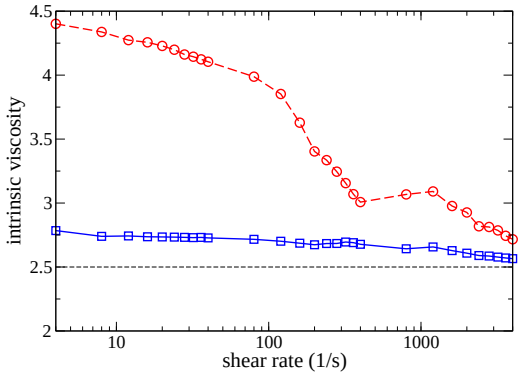


FIG. 6. The intrinsic viscosity as a function of the shear rate. Solid lines with squares correspond to the inactive swimmer. Dashed lines with circles correspond to the active swimmer.

of the swimmer ($L/(8\pi\eta R^3)$) normalized by the angular velocity of a sphere due to the shear flow ($-\dot{\gamma}/2$). Here $L$ is the torque applied on the central bead by one of the following: the main springs; the supporting springs; all spring together or all springs and shear flow (the total torque).

Figure 5(I) describes the configuration where the flagella plane and the swimming direction are perpendicular to the flow. Due to the shear flow, the body of the swimmer is rotating with an angular velocity $-\dot{\gamma}/2$. If the tangent velocity of small beads (along $x$) is $v_1 = -\dot{\gamma}\widetilde{\ell}_y/2$ swimmer would rotate without deformation. Here $\widetilde{\ell}_y$ is the distance between the central bead and the small beads along $y$. However, the velocity gradient of the shear flow between those beads is $v_2 = -\dot{\gamma}\widetilde{\ell}_y$. The difference between those two velocities regularly deforms swimmer clockwise in the shear plane. The main springs of the freely moving swimmer without an external flow does not apply a force on beads out of the shear plane. In a shear flow, main springs of deformed swimmer apply forces on central beads that have nonzero $x$ components [Fig. 5(I)] and therefore exerts a torque on the central bead. Figure 5(a) shows the actual lengths of the main springs ($\ell$) and the time-dependent equilibrium length of main springs ($\ell_m$) during the orbital period of small beads. When the main springs are compressed ($\ell < \ell_m$) the torque exerted by the main springs to the central bead is opposite of the torque applied by the shear flow. Meanwhile, the supporting springs exerts a torque on the central bead which have the same sign as the torque applied by the shear flow. However, the total torque exerted by all springs on the central bead is opposite of the one applied by the shear flow. Therefore, the rotation of swimmer by the flow is reduced, and swimmer stays longer in given configuration (perpendicular to the flow). Such behavior is opposite of a passive elongated object in a shear flow (Jeffrey's Orbit) [34].

In contrast, when the flagella plane is perpendicular to the flow and swimming direction is parallel to the flow [see Fig. 5(II)] the swimmer deforms in the opposite way.

The shear flow rotates the body of a swimmer with angular velocity $-\dot{\gamma}/2$. The velocity needed for a small bead without deforming swimmer is again $v_1 = -\dot{\gamma}\widetilde{\ell}_y/2$. However, the velocity gradient of the shear flow between central and small beads is zero ($v_2 = 0$). Therefore, swimmer deforms counter-clockwise. The total torque exerted by all springs on the swimmer amplifies the rotation imposed by the flow. The swimmer makes a rapid flip [compare Fig. 5(I.c) and Fig. 5(II.c)]. for the changing the orientation angle). Note that leading effect for exerting the torque and changing of rotation speed comes from the main springs (which together with the small beads imitate flagella) and the supporting springs only reduce the effect. Therefore, we expect a similar behavior for the prototype *CR* swimmer. However, further experiments are required to examine dynamics of the *CR* under the flow.

When the flagella plane and the shear plane is common, each spring exerts a torque on the swimmer such that it equalizes the rotation velocity, and the angular orbit is almost linear [see Fig. 3(a)].

We calculated the intrinsic viscosity for a wide range of shear rates and found the shear thinning behavior also reported in previous experiments [9] [see Fig. 6]. We found shear thinning typical for the suspension of a deformable elastic object (e.g. the red blood cells [35]) for the active swimmer suspension. Obtained complex shear thinning profile of active swimmer suspension is related to the existence of two timescales: small beads orbiting period $T_b$ and the tumbling period in the flow $T$. If $T/T_b > 100$ the effect of the altering angular orbits is important and contributes to the viscosity enhancement for the active swimmers, In higher shear rates the effect vanishes. However, if we consider even smaller shear rates the effect does not increase significantly since the flow becomes weaker to deform the swimmer.

## V. CONCLUSION

A three-dimensional model has been developed for *Chlamydomonas Reinhardtii* that takes into account flagellar beating. The model correctly reproduces most of the swimming characteristics of studying microswimmer. Using the model, we found a reversed Jeffrey's like orbit for the microswimmer in the shear flow. Such an altered orbit gives rise to the enhancement of suspension viscosity. However, the main enhancement of the active swimmer viscosity is related to the effectively enlarged shape of the active swimmers due to the flagellar beating.

We estimate the intrinsic viscosity for the active swimmer suspension and the inactive swimmer suspension using numerical simulations within the generalized Rotne-Prager approximation. The results for the intrinsic viscosity are compared with our previous experimental measurements [9], also confirmed by another experiment with a different geometry by Mussler *et al.* [10] and we found good agreement. We also found a shear thinning behavior for the active swimmer suspensions.

The results suggest that significantly increased viscosity for puller-type active microswimmer suspensions can be explained by considering the activity of an individual swimmer without a collective behavior. However, the interaction between swimmers (i.e. collective effects) can be significant in concentrated suspensions.

The complex angular orbits of the model swimmer and its consequences to the suspension viscosity for different orientations of the swimmer with respect of the flow direction, emphasize the importance of using a three-dimensional model for such a system.


[1] E. Lauga and T. R. Powers, Rep. Prog. Phys. **72**, 096601 (2009).
[2] R. Dreyfus, J. Baudry, M. L. Roper, M. Fermigier, H. A. Stone, and J. Bibette, Nature **437**, 862 (2005).
[3] E. E. Keaveny and M. R. Maxey, J. Fluid Mech. **598**, 293 (2008).
[4] N. Casic, N. Quintero, R. Alvarez-Nodarse, F. Mertens, L. Jibuti, W. Zimmermann, and T. Fischer, Phys. Rev. Lett. **110**, 168302 (2013).
[5] E. M. Purcell, Am. J. Phys. **45**, 3 (1977).
[6] B. Kaoui, G. Ristow, I. Cantat, C. Misbah, and W. Zimmermann, Phys. Rev. E **77**, 021903 (2008).
[7] Y. Hatwalne, S. Ramaswamy, M. Rao, and R. Simha, Phys. Rev. Lett. **92**, 118101 (2004).
[8] A. Sokolov and I. Aranson, Phys. Rev. Lett. **103**, 148101 (2009).
[9] S. Rafaï, L. Jibuti, and P. Peyla, Phys. Rev. Lett. **104**, 098102 (2010).
[10] M. Mussler, S. Rafaï, P. Peyla, and C. Wagner, Eur. Phys. Lett. **101**, 54004 (2013).
[11] W. M. Durham, J. O. Kessler, and R. Stocker, Science **323**, 5917 (2009).
[12] J. Gachelin, G. Miño, H. Berthet, A. Lindner, A. Rousselet, and E. Clément, Phys. Rev. Lett. **110**, 268103 (2013).
[13] D. Saintillan, Phys. Rev. E **81**, 056307 (2010).
[14] B. M. Haines, *Effective Viscosity of Dilute Bacterial Suspensions*, Ph.D. thesis, The Pennsylvania State University (2011).
[15] S. Heidenreich, S. Hess, and S. Klapp, Phys. Rev. E **83**, 011907 (2011).
[16] Z. Cui, Phys. Rev. E **83**, 031911 (2011).
[17] B. M. Haines, I. S. Aranson, L. Berlyand, and D. A. Karpeev, Phys. Biol. **5**, 046003 (2008).
[18] C. Brennen and H. Winet, Annu. Rev. Fluid Mech. **9**, 339 (1977).
[19] J. P. Hernandez-Ortiz, P. T. Underhill, and M. D. Graham, J. Phys.: Condens. Matter **21**, 204107 (2009).
[20] V. Mehandia and P. R. Nott, J. Fluid Mech. **595**, 239 (2008).
[21] K. Drescher, R. Goldstein, N. Michel, M. Polin, and I. Tuval, Phys. Rev. Lett. **105**, 168101 (2010).

[22] R. Bennett and R. Golestanian, Phys. Rev. Lett. **110**, 148102 (2013).
[23] B. Friedrich and F. Jülicher, Phys. Rev. Lett. **109**, 138102 (2012).
[24] M. Garcia, S. Berti, P. Peyla, and S. Rafaï, Phys. Rev. E **83**, 035301 (2011).
[25] E. H. Harris, *The Chlamydomonas sourcebook: introduction to Chlamydomonas and its laboratory use*, Vol. 1 (Academic Press, 2009).
[26] J. Happel and H. Brenner, *Low Reynolds number hydrodynamics*, Vol. 1 (Springer, 1983).
[27] A. Einstein, Ann. Phys. (Leipzig) **19**, 289 (1906).
[28] G. K. Batchelor and J. T. Green, J. Fluid Mech. **56**, 401 (1972).
[29] L. D. Landau and E. M. Lifshitz, *Fluid Mechanics: Landau and Lifshitz: Course of Theoretical Physics*, edited by Pergamon (Pergamon, 2nd edition, 1987).
[30] A. S. Sangani, A. Acrivos, and P. Peyla, Phys. of Fluids (1994-present) **23**, 083302 (2011).
[31] I. M. Kreiger and T. J. Dougherty, Trans. Soc. Rheol. **3**, 137 (1959).
[32] J. Rotne and S. Prager, J. Chem. Phys. **50**, 4831 (1969).
[33] E. Wajnryb, K. A. Mizerski, P. J. Zuk, and P. Szymczak, J. Fluid Mech. **731**, R3 (2013).
[34] G. B. Jeffery, Proc. R. Soc. London **102**, 161 (1922).
[35] A. M. Forsyth, J. Wan, P. D. Owrutsky, M. Abkarian, and H. A. Stone, Proc. Natl. Acad. Sci. **108**, 10986 (2011).